iScience

CellPress
OPEN ACCESS

Article

Immune-mediated neurodegenerative trait provoked by multimodal derepression of long-interspersed nuclear element-1

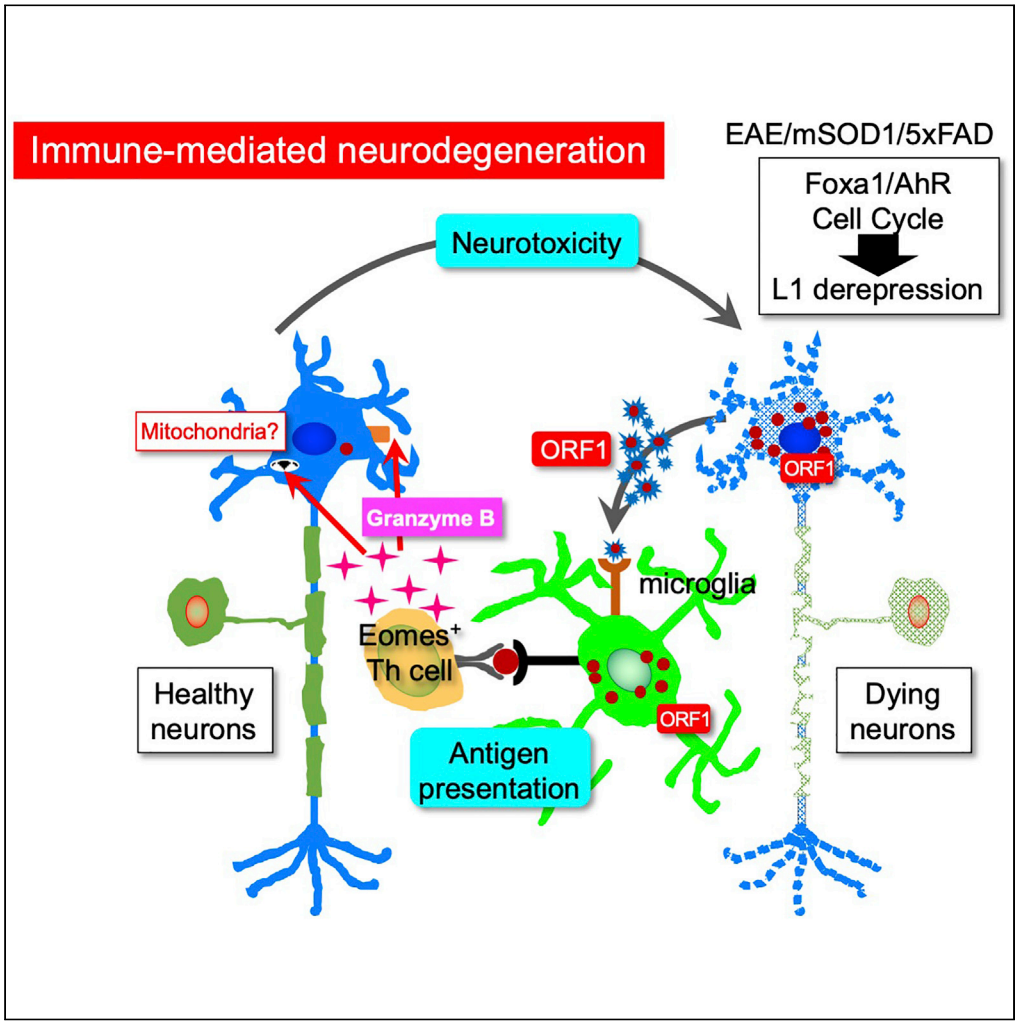

Fumio Takahashi, Chenyang Zhang, Hirohiko Hohjoh, Ben Raveney, Takashi Yamamura, Nobuhiro Hayashi, Shinji Oki

soki@ncnp.go.jp

Highlights

Eomes + Th cells accumulate in the CNS with undergoing neurodegeneration in common

Multimodal L1 derepression is emerged in neuron cells under neurodegeneration

Eomes + Th cells recognize L1-ORF1 antigen to exert neurotoxicity via granzyme B

Immune-mediated neurotoxicity may embody a novel pathogenesis of neurodegeneration

Takahashi et al., iScience 25, 104278
May 20, 2022
https://doi.org/10.1016/j.isci.2022.104278

iScience

CellPress
OPEN ACCESS

Article

Immune-mediated neurodegenerative trait provoked by multimodal derepression of long-interspersed nuclear element-1

Fumio Takahashi,[1,3] Chenyang Zhang,[1] Hirohiko Hohjoh,[2] Ben Raveney,[1] Takashi Yamamura,[1] Nobuhiro Hayashi,[3] and Shinji Oki[1,4,*]

SUMMARY

Neurodegeneration is a process involving both cell autonomous and non-cell autonomous neuron loss, followed by a collapse of neural networks, but its pathogenesis is poorly understood. We have previously demonstrated that Eomes-positive helper T (Eomes + Th) cells recognizing LINE-1(L1)-derived prototypic antigen ORF1 mediate neurotoxicity associated with the neurodegenerative pathology of experimental autoimmune encephalomyelitis (EAE). Here, we show that Eomes + Th cells accumulate in the CNS of mouse models of authentic neurodegenerative diseases, including amyotrophic lateral sclerosis (ALS) and Alzheimer's disease (AD), and secrete the neurotoxic granzyme B after encounter with ORF1 antigen. Multimodal derepression of neuronal L1 transcription is observed in EAE and ALS/AD models during neurodegeneration in active and cell cycle-mediated manner, respectively. These data suggest that the adventitious concurrence of immune-mediated neurodegenerative traits by Eomes + Th cells and ectopic expression of L1-derived antigen(s) in the inflamed CNS may materialize a communal and previously unappreciated pathogenesis of neurodegeneration.

INTRODUCTION

Neurodegeneration is the process of structural or functional failure and the subsequent death of neurons (Przedborski et al., 2003). This is a common and shared process of various neurodegenerative diseases (NDs), including amyotrophic lateral sclerosis (ALS), Alzheimer's disease (AD), and Parkinson's disease (PD). Following identification of a series of risk factors, NDs are regarded as proteinopathies, each with unique protein aggregates observed in individual diseases (Raine, 2000). Recent works have proposed a non-cell autonomous mechanism for pathogenesis of NDs, which is associated with dysregulation of microglia and astrocytes (Seol et al., 2020; Van Harten et al., 2021). In particular, aberrant glial activation has been linked to neurodegeneration, which induces chronic neuroinflammation and recruits miscellaneous immune cells into the CNS, thus compromising immune homeostasis (Ciccocioppo et al., 2020). As these diverse NDs share many similar characteristics despite differences in precise symptoms and the identity of the protein aggregates, it is conceivable that some or all of these NDs result from a common pathogenesis based on dysregulated immune responses. Yet, to date little progress has been made in examining the pathogenic relevance of immune responses spanning diverse NDs. Therefore, it remains unclear whether or not atypical functionality of certain immune responses *per se* is intrinsically pathogenic to general neurodegeneration and such detailed research may provide previously unappreciated perspectives for the pathogenesis of ND.

The process of neurodegeneration in itself is not exclusively observed in NDs; many inflammatory CNS diseases are also accompanied by symptomatic or asymptomatic neurodegeneration. For example, secondary progressive multiple sclerosis (SPMS) which is typified by neurodegeneration-like pathology manifests after a preceding immune-driven course of demyelination (Rovaris et al., 2006). In SPMS, pathological symptoms of neurodegeneration and axonal dysfunction are apparent and these hallmarks significantly overlap with those of general NDs (Correale et al., 2017). SPMS pathogenesis has been recently revised from a purely neurodegenerative disease, to one co-linked to chronic inflammation mediated by immune

[1]Department of Immunology, National Institute of Neuroscience, NCNP, Tokyo, Japan

[2]Department of Molecular Pharmacology, National Institute of Neuroscience, NCNP, Tokyo, Japan

[3]School of Life Science and Technology, Tokyo Institute of Technology, Tokyo, Japan

[4]Lead contact

*Correspondence: soki@ncnp.go.jp

https://doi.org/10.1016/j.isci.2022.104278

cells. For example, a selective sphingosine-1-phosphate receptor (S1PR) modulator, Siponimod, which modulates the function of lymphocytes (Wu et al., 2020), has been shown to be an effective treatment in (Kappos et al., 2018). Furthermore, we have previously identified a cytotoxic-like helper T cell subset infiltrating the CNS of SPMS patients and its animal model, experimental autoimmune encephalomyelitis (EAE) (Raveney et al., 2015, 2021). These Eomes-expressing helper T cells (Eomes + Th cells) were able to act as an authentic agitator of neurotoxicity in EAE. In SPMS, Eomes + Th cells correlated significantly with the degree of disability progression (Raveney et al., 2021), implying that pathogenic T cell populations play a key role in the neurodegenerative process of SPMS.

Disease-associated microglia (DAM) have been identified in ND models, including amyloid-β-mediated and tau-mediated AD mouse models, an ALS model, etc (Deczkowska et al., 2018). Similar DAM are also observed in postmortem AD brains (Keren-Shaul et al., 2017). DAM maintain the expression of typical microglial markers such as Iba1, but have downregulated typical homeostatic markers of microglia such as P2ry12, P2ry13, and Cx3cr1. Instead, DAM have increased expression of genes that are known as AD risk factors, including genes involved in lysosomal, phagocytic, and lipid metabolism pathways such as Apoe, Tyrobp, and Trem2. Importantly, upregulated gene sets include factors involved in antiviral and interferon response genes and MHC class II components (Mathys et al., 2017), indicating that the immunological characteristics of DAM may be involved in the pathogenesis of neurodegenerative diseases. The presence of microglia with a phenotype showing enhanced type-I interferon (IFN-I) signature and MHC class II (MHC II) expression in EAE prompted us to hypothesize that these activated microglia may be acting as antigen-presenting cells to drive Eomes + Th cell activation. We have shown that cytotoxic-like Eomes + Th cells produce granzyme B on activation (Raveney et al., 2015), which can in turn drive neurodegeneration directly. The most interesting question of this proposed pathogenic mechanism is that this process would be the nature of the putative antigen(s) presented in the context of microglial MHC class II that initiate these immune responses.

Similar exploration of putative antigen(s) has long been carried out in the field of tumor immunology. For example, endogenous retroelements are getting considerable attention as a potential class of alternative tumor-specific antigens (Smith et al., 2019). Interestingly, dysregulated increase of endogenous retroelements has also been associated with NDs (Peze-Heidsieck et al., 2021; Ravel-Godreuil et al., 2021): high levels of expression and reactivation of retrotransposable element, LINE-1 (Long interspersed nuclear element 1, L1), in postmortem brain samples of ALS and FTD ALS in TDP-43 (TAR DNA-binding protein of 43 kDa)-dependent manner (Liu et al., 2019; Tam et al., 2019). Thus, aberrant expression of endogenous retroelement under chronic inflammation could provide the currently unknown antigen(s) that may prime Th cell in the CNS.

An approximately half of the human genome is composed of retrotransposable elements (RE) with more than 30% of these being LINE1 which manifest as half million copies in the human genome (Cristofari, 2017); 80-100 copies of human L1 and 3000 copies of mouse L1 are retrotransposable. L1 retrotransposition under neurogenesis has been shown to lead to neuronal genome diversity and somatic mosaicism in the developing brain (Thomas et al., 2012). Meanwhile, dysregulated L1 insertion potentially compromises developing and mature neurons and so may cause neurodevelopmental diseases and neurodegenerative diseases (Nicole et al., 2017). Interestingly, L1 activation has been frequently highlighted as a comorbidity in NDs (Peze-Heidsieck et al., 2021; Ravel-Godreuil et al., 2021). However, comprehensive analysis of the mode of L1 activation and its relevance to neuronal cell death remains to be investigated. As dysregulated L1 expression was reported to be associated with loss of nuclear TDP-43 in postmortem brain samples of ALS patients (Liu et al., 2019; Tam et al., 2019), we set out to examine whether derepression of L1, which encode two proteins, ORF1 and ORF2, may provide a previously unappreciated pathogenic mechanism of general neurodegeneration via immune-mediated neurotoxicity. By employing independent animal models of NDs, we now demonstrate that an immune-mediated neurodegenerative trait commonly underlies in diverse NDs and multimodal derepression of neuronal L1 provokes those Th cells infiltrating into CNS to secrete neurotoxic granzyme B.

RESULTS

Eomes$^+$ Th cells preferentially accumulate in the CNS of mSOD1 or 5xFAD mice

We have previously observed that Eomes + Th cells accumulate in the CNS of late EAE and SPMS patients and can act to drive neurotoxicity via secretion of granzyme B (Raveney et al., 2015, 2021). Furthermore, we

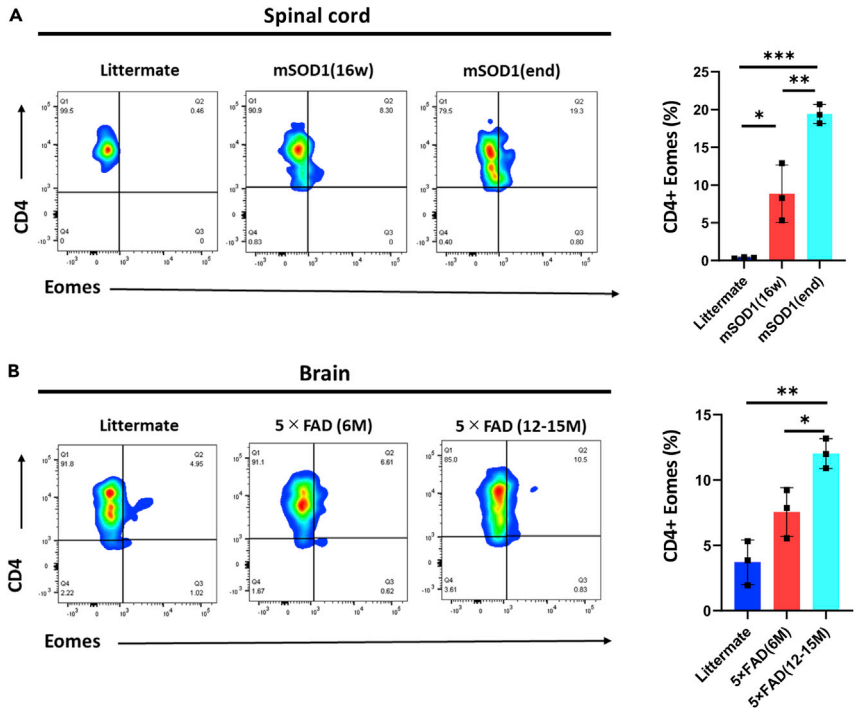

Figure 1. Eomes + Th cell accumulation in the CNS of mSOD1 or 5xFAD mice

(A) Mononuclear cells isolated from SC of 16w and end stage mSOD1 mice and 16w littermate were stained with anti-CD45, anti-TCRβ, anti-CD4, and anti-Eomes Ab, and were then analyzed by using flow cytometer. Typical plots and representative summary data (n = 3) of three independent experiments with similar results are shown.

(B) Mononuclear cells isolated from the brain or SC of 12 and 15M 5xFAD mice and 12M littermate were stained with anti-CD45, anti-TCRβ, anti-CD4, and anti-Eomes Ab, and were then analyzed by using flow cytometer. Typical plots and representative summary data (n = 3) of three independent experiments with similar results are shown. Statistical analysis was performed by one-way ANOVA with Bonferroni's multiple comparison.

found that the chronic neuroinflammatory milieu played a pivotal role in Eomes + Th cell development in the CNS (Zhang et al., 2019). As most ND are closely associated with chronic inflammation, attracting immune cells into the CNS and modulating immune cell function (Ciccocioppo et al., 2020), we evaluated immune cell infiltration in the CNS of two independent mouse models of neurodegeneration, mSOD1 and 5×FAD. As shown in Figure 1A, Eomes + Th cells were significantly increased in the spinal cord (SC) of 16w-old mSOD1 mice compared with presymptomatic 12w-old mice. Greater increases in Eomes + Th cells were observed in end stage disease (~21w), suggesting a correlation between disease severity and Eomes + Th cells infiltration. Similarly, there was a gradual increase of Eomes + Th cells in the brain of 6 months-old 5xFAD mice over control littermate, which became significant after disease was fully established (12–15-months old, Figure 1B). Primary lesion formation in 5xFAD mice begins in a relatively limited area of the memory system in the medial temporal lobe, such as in the hippocampus and the entorhinal cortex. Thus, we could only detect significant accumulation of Eomes + Th cells after neurodegenerative lesions had expanded into the whole brain in this model. To confirm the functional significance of moderate Eomes expression in Th cells in neurodegenerative disease models, we compared granzyme B expression between CNS Th cells from 5xFAD mice and granzyme B-deficient 5xFAD mice. As shown in Figure S1, all granzyme B-positive Th cells formed part of the Eomes + subset, and although granzyme B expression was abolished in granzyme B-deficient 5xFAD mice, the frequency of Eomes + Th cells was maintained. Therefore, moderate Eomes expression because of milder net inflammatory responses in the CNS of mSOD1 and 5xFAD mice does not necessarily impair their functional significance as a pathogenic component.

L1-ORF1 expression is upregulated in the SC neurons of EAE mice

We hypothesized that peptides from RE could act as putative peptides to drive Eomes + Th cell activation. As late EAE, mSOD1, and 5xFAD all were associated with Eomes + Th cells in the CNS and all show neurodegenerative symptoms, we aimed to investigate the neuronal induction of ORF1 expression in individual

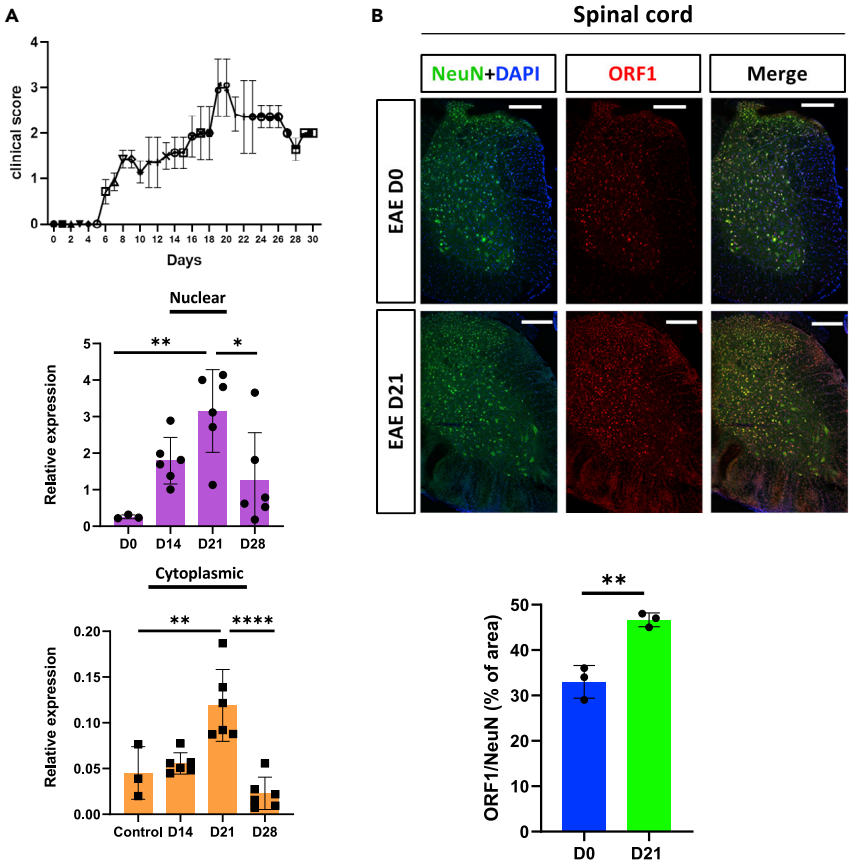

Figure 2. Induction of L1-ORF1 expression in SC neurons of EAE mice

(A) B_6 mice were immunized with MOG35–55 peptide on days 0 and with PT on days 0 and 2, and clinical scores were daily evaluated. Representative clinical scores for EAE are shown (in upper panel). Representative data (n = 6) of more than five independent experiments with similar results are shown as the mean ± SEM (In middle and lower panels) Nuclear and cytoplasmic RNAs were extracted from SC neurons on day 0, 14, 21, and 28 after EAE induction and L1 transcripts were quantified by qRT-PCR as described in the STAR Methods. Representative data (n = 3 or 6) of more than three independent experiments with similar results are shown as the mean ± SD. *, $p < 0.05$; **, $p < 0.01$; ***, $p < 0.001$; ****, $p < 0.0001$ hereafter by one-way ANOVA with Bonferroni's multiple comparison.

(B) Immunofluorescence images of SC section (control vs EAE at day 21) stained with anti-NeuN Ab (Green), anti-ORF1 Ab (Red) and DAPI (Blue). Bars, 200 μm. Relative frequency of ORF1-expressing cells within NeuN + neurons in the gray matter were quantified based on microscopic observation and automated cell counting on three different sections. Representative data of three independent experiments with similar results are shown.

mouse models. Nucleocytoplasmic shuttling of L1 transcript occurs during ribonucleoprotein complex assembly; therefore, to address this, we were quantified nuclear and cytoplasmic RNAs separately. L1 transcripts were significantly increased in the nucleus and cytoplasm at day 21 with some upregulation of nuclear transcripts at day 14 after EAE induction (Figure 2A). Interestingly, L1 transcript is quickly decreased at day 28, suggesting that L1 could temporally be upregulated even under strict control. Furthermore, immunofluorescence imaging analysis revealed that ORF1 protein expression is increased in neurons in SC gray matter. Quantitative analysis revealed a significant increase of ORF1-expressing neurons in the SC of EAE mice (Figure 2B). Interestingly, we observed the induction of ORF1 protein expression in cells distributed through white matter, indicating an enhanced expression of ORF1 in glial cells after EAE induction. These results demonstrate that both L1 transcript and ORF1 protein are upregulated in SC neurons after the induction of EAE.

Multiple signaling pathways are involved in transient induction of L1 expression

As retroelements including L1 are thoroughly heterochromatinized to suppress their expression and downstream genotoxic effects, most somatic cells show no or little expression of retroelements under

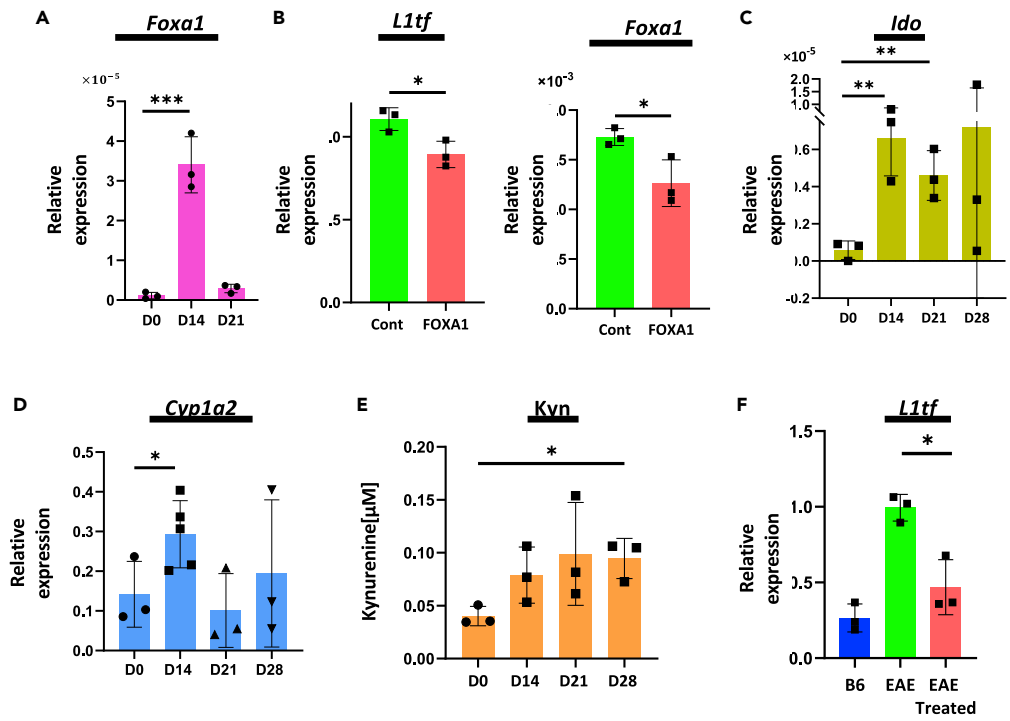

Figure 3. Chromatin relaxation and Ahr signals in acute L1 upregulation in SC neurons of EAE mice

(A) Expression levels of Foxa1 were quantified by qRT-PCR in SC neurons after EAE induction (n = 3). Representative data of three independent experiments with similar results are shown. Data represent the mean ± SD. Statistical analysis was performed by unpaired Student's *t* test against day 0. *, $p < 0.05$; **, $p < 0.01$; ***, $p < 0.001$; ****, $p < 0.0001$.

(B) SC neurons isolated from EAE mice at day 21 were cultured for 24h, and expression levels of Foxa1 and L1 were quantified 48 and 72h after treatment with Foxa1-specific siRNA or scrambled control RNA, respectively. Representative data of three independent experiments with similar results are shown. Values represent the mean ± SD. Statistical analysis was performed by unpaired Student's *t* test.

(C) Relative expression of Ido in SC neurons of EAE mice was determined by qRT-PCR. Representative data of three independent experiments with similar results are shown. Data represent the mean ± SD. Statistical analysis was performed by unpaired Student's *t* test against day 0.

(D) Relative expression of Cyp1a2 in SC neurons of EAE mice was determined by qRT-PCR. Representative data of three independent experiments with similar results are shown. Data represent the mean ± SD. Statistical analysis was performed by unpaired Student's *t* test against day 0.

(E) Levels of kynurenine concentration extracted from the whole SCs were quantified. Representative data of two independent experiments with similar results are shown. Data represent the mean ± SD. Statistical analysis was performed by unpaired Student's *t* test against day 0.

(F) Mice were treated with 1-MT or vehicle daily from day 7–11 after EAE induction, and SC neurons were harvested at day 14. Relative expressions of L1 in intact, vehicle-treated, or 1-MT-treated EAE mice are shown. Representative data (n = 3) of two independent experiments with similar results are shown. Statistical analysis was performed by unpaired Student's *t* test.

physiological conditions. To explore how L1 is derepressed in neuronal cells during EAE, we first investigated three factors that are associated with L1 regulators in aging cells, Foxa1, Rb1, and Trex1 (De Cecco et al., 2019). Transcription of Foxa1, a pioneer transcription factor that induces relaxation of chromatin structure allowing access by other transcription factors, was significantly increased in the induction phase of EAE (day 14) and was abolished around the peak of the disease (Figure 3A). This finding correlated with the induction of Foxa1 protein observed in SC neurons of EAE mice (Figure S2). Meanwhile, little increase of Rb1 and Trex1 expression was observed, although there was a tendency for upregulation at later stages (Figure S3). Primary neurons isolated from SC on day 14 EAE were transfected with Foxa1-specific siRNA and this treatment reduced L1 induction as well as Foxa1 expression (Figure 3B). Importantly, Foxa1-specific siRNA also inhibited Foxa1 protein expression in SC neurons as well (Figure S4), suggesting that Foxa1-mediated chromatin relaxation is involved in L1 upregulation in EAE neurons.

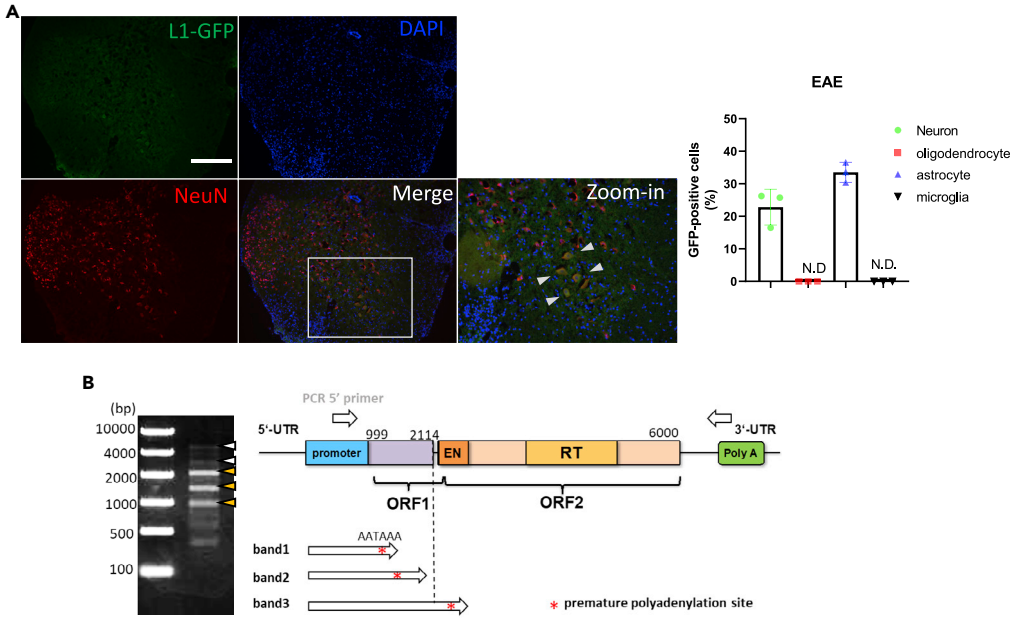

Figure 4. L1 retrotransposition and predominant accumulation of truncated transcript in SC neurons of EAE mice

(A) SC obtained from L1-GFP mice 21 days after EAE induction were stained with anti-NeuN Ab and DAPI. Cells experiencing retrotransposition are visualized with GFP. (Inset) Fluorescence image of GFP + neurons with higher magnification (white arrowheads). Representative data of 3 independent experiments with similar results are shown. Bars, 200 μm. Relative frequency of GFP + cells were quantified in neurons and glial cells in SC of EAE mice.

(B) RNA extracted from SC neurons 21 days after EAE induction were reverse-transcribed with oligo dT primes and cDNAs were amplified by conventional PCR with ORF1 sense primer and oligo dT primers as shown in open white arrows. Three dominant short transcripts between 1 and 2kb (band 1 to 3, yellow arrowheads) and two longer transcripts (white arrowheads) were amplified. Relative extension of three dominant transcripts and the corresponding locations within L1 gene were shown in open arrows with identified polyadenylation sites in red asterisks. Representative data of 3 independent experiments with similar results are shown.

L1s are upregulated via activation of the aryl hydrocarbon receptor (AhR) pathway after exposure to environmental polycyclic aromatic hydrocarbons (Okudaira et al., 2010; Teneng et al., 2007). Kynurenine is an endogenous AhR ligand that is converted from tryptophan by indoleamine 2,3-dioxygenase (Ido). Ido has been reported to be upregulated during EAE (Kwidzinski and Bechmann, 2007) and we observed that Ido upregulation in EAE correlated with Cyp1a2 upregulation (Figures 3C and 3D), a typical target gene of AhR activation. Accordingly, kynurenine was increased in SC at day 14 after EAE induction and was maintained thereafter (Figure 3E). Importantly, intraperitoneal injection of EAE mice with a competitive inhibitor of Ido (1-methyl tryptophan; 1-MT) significantly suppressed L1 expression in SC neurons (Figure 3F). As Ido inhibition to reduce L1 expression could act via reduced AhR activation, our results as a whole suggest that induction of Foxa1 and activation of AhR signaling pathway are synergistically involved in relaxing of L1-associated heterochromatin and active induction of L1 transcription, respectively, in SC neurons during EAE. However, our data does not exclude the possibility that other metabolite(s) downstream of multifaceted tryptophan metabolic pathways could provide compensatory or off-target effects.

Short L1 transcripts are preferentially expressed in SC neurons of EAE mice

L1 is the only retrotransposable element (RTE) that retrotransposes autonomously in the human genome. L1 retrotransposition promotes aberrant transcription, alternative splicing, insertional mutagenesis, DNA damage and genome instability that causes many CNS diseases (Kazazian and Goodier, 2002). Therefore, we examined L1 retrotransposition in the SC of EAE mice to explore whether ORF1 upregulation in SC neurons is quantitatively correlated with retrotransposition. For this purpose, we induced EAE in L1-GFP reporter mice and analyzed GFP expression in SC sections. Although there some GFP is observed in SC neurons after EAE induction, which preferentially overlaps with anterior horn neurons (Figure 4A), there is a broad distribution of GFP(−)/ORF1(+) neurons in the gray matter. Importantly, significant numbers of neurons and astrocytes were GFP positive, whereas little GFP was detected in oligodendrocytes and microglia

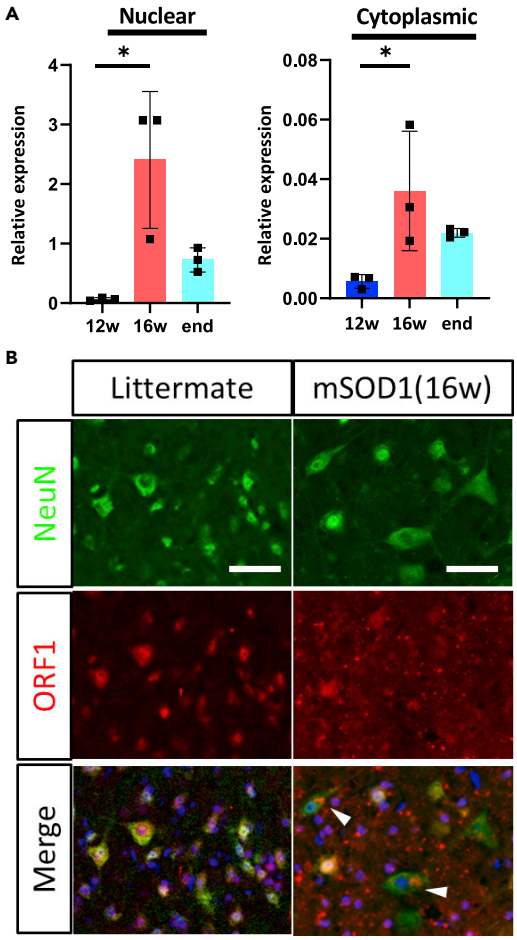

Figure 5. Induction of L1-ORF1 expression in SC neurons of mSOD1 mice

(A) Nuclear and cytoplasmic RNAs were purified from SC neurons of 12w, 16w and end stage (over 21-wks old) mSOD1 mice and L1 transcripts were quantified as shown in Figure 2. Representative data (n = 3) of three independent experiments with similar results are shown as the mean ± SD. Statistical analysis was performed by one-way ANOVA with Bonferroni's multiple comparison. *, $p < 0.05$; **, $p < 0.01$; ***, $p < 0.001$; ****, $p < 0.0001$.

(B) Immunofluorescent images of ORF1 expression in SC sections of mSOD1 mice. Sections obtained from SC of 16w mSOD1 mouse were stained with anti-NeuN Ab (Green), anti-ORF1 Ab (Red), and DAPI (Blue). White arrowheads indicate intracellular/perinuclear aggregate formation of ORF1. Representative data of three independent experiments with similar results are shown. Bars, 200 μm.

(Figure 4A). These results suggest that ORF1 signals detected in EAE SC white matter are most likely resulted from astrocytes (Figure 2C). Next, we examined whether the upregulated L1 transcription was extended to the 3′ end, providing full length L1 genes. By using a set of 5′UTR primer and oligo dT primer, we detected three major products of 1∼2kb length and two faint longer products, the longest of which seems to correspond to the full length L1 RNA (∼6kb) (Figure 4B, left panel). The three short products were confirmed to encode truncated L1 transcripts due to premature polyadenylation. Among them, the longest transcript covered the open reading flame of the ORF1 gene (Figure 4B, right panel).

These data suggest that a congenital protective mechanism of premature polyadenylation significantly restricts the full transcription of L1 gene, resulting in the dominant expression of ORF1-encoding transcripts.

L1-ORF1 expression is induced in SC neurons of mSOD1 mice

Next, we analyzed the neuronal induction of L1-ORF1 expression in mSOD1 mice. L1 transcripts were at a low level in the SC of presymptomatic 12weeks-old mice, then increased in both nucleus and cytoplasm by 16 weeks old and decreased gradually by end stage disease (∼21w) (Figure 5A). Although L1 expression

was quickly abolished one week after peak EAE disease, L1 expression was maintained until the end stage of mSOD1 disease, suggesting that an alternative regulatory mechanism governs L1 expression in mSOD1 mice. Immunofluorescence imaging analysis showed that many SC neurons in 16 week-old mSOD1 mice were damaged, but intracellular and extracellular ORF1 protein signals were increased in the SC neurons of 16 week-old mSOD1 mice compared with those of littermate controls. Interestingly, some surviving neurons showed ORF1 intracellular/perinuclear aggregate formation. Although ORF1 is a typical RNA binding protein that interacts with many cellular transcripts (Kolosha and Martin, 2003), further study is required to elucidate the mechanism of ORF1 aggregate formation. Taken together, these results demonstrate that both L1 transcript and ORF1 protein are upregulated in SC neurons in the mSOD1 mouse during disease.

Upregulation of neuronal L1 expression is associated with temporal cell cycle progression

Cell cycle-related factors are upregulated in various neurodegenerative diseases (Joseph et al., 2020) and dysregulated cell cycle progression has been reported in postmitotic neurons. Such unusual cell cycle progression allows the generation of hyperploid neurons that go beyond the G_1/S checkpoint and are implicated in the pathogenesis of neurodegenerative disease. Rb protein binds repetitive sequences in somatic cells and maintains a H3K27me3-dependent repression of retroelements via RB-EZH2 complexes in a cell cycle-independent manner (Ishak et al., 2016). Rb1 transcripts were exclusively increased in neurons of 16 week-old mSOD1 mice and maintained until the end stage of the disease (Figure S5). Furthermore, there are significant numbers of neurons with cytoplasmic phosphorylated Rb1 (pRb1) in mSOD1 mice (Figure S6). Interestingly, Iba-1+ microglia and olig2+ oligodendrocytes, but not GFAP + astrocytes provided some pRb1 signals, suggesting that some of those glial cells in diseased mSOD1 mice are also in cell cycle progression (Figure S6).

When we examined the cell cycle status of SC neurons from non-diseased and diseased mSOD1 mice, we observed neurons from mSOD1 mice were distributed more to S and G_2/M phase than neurons from non-diseased mice that were composed mostly of cells in G_0/G_1 phase (Figures 6A and S7). Although the relative frequency of neurons in cell cycle progression is comparable with that of healthy mature adult human neurons or those during neurodegenerative disease (Pack et al., 2005), immunohistochemical analysis of Cdt1 and geminin expression indicated that SC neurons from mSOD1 mice showed exclusive cell cycle progression that occurred much earlier than the onset of neurodegeneration (Figure S8). Quantitative analysis of L1 expression after sorting of neurons in each cell cycle phase revealed that L1 expression is significantly higher in S to G_2/M phase neurons than G_0/G_1 phase neurons and mSOD1 neurons showed a more skewed L1 expression in association with cell cycle progression (Figure 6B). As shown in Figures 6A and 6B net L1 expression level in the neurons of individual cell cycle phases demonstrated that neurons in G_2/M phase are the most remarkable source of L1 products (Figure 6C) and G_0/G_1 neurons derived from mSOD1 mouse expressed significantly lower L1 products than by intact neurons. It should be noted that the level of ORF1 transcripts is much higher than ORF2 transcripts, implying that the suppressive machinery that limits the extension of transcription observed in late EAE neurons may also be in operation. Accordingly, some GFP-positive neurons and GFP-positive oligodendrocytes were detected in 10 week-old L1-GFP/mSOD1 mice (Figure S9). Therefore, the pathogenic involvement of L1 retrotransposition in neurons and glia awaits further investigation.

Next, immunofluorescence imaging analysis revealed that spinal anterior horn cells obtained from pre-symptomatic (10-week old) mSOD1 mice showed higher expression of cytoplasmic cyclin D1 and CDK4 (Figure 6D); their punctate immunoreactivities resemble those observed in SC motor neurons of ALS patients (Ranganathan and Bowser, 2003). Interestingly, immunoreactivities to cyclin D1 and CDK4 significantly overlapped with that of ORF1, indicating that they may form a complex in mSOD1 neurons. These results suggest that neurons in the mSOD1 mouse are prone to enter cell cycle, which may allow ectopic L1 expression in those neurons.

CNS Th cells associated with neurodegeneration secrete granzyme B after exposure to ORF1 protein

As we have shown that granzyme B production by populations of cytotoxic-like Th cells in CNS result in damage to surrounding neurons, we examined whether ORF-induced priming could drive of CNS Th cells from late EAE, mSOD1, and 5xFAD mouse to secrete granzyme B. CNS Th cells or splenic Th cells isolated from EAE mice (day28) were cocultured with bone-marrow-derived dendritic cells (BMDC) preloaded with or without ORF1 and granzyme B-secreting Th cells were quantified by using an enzyme-linked

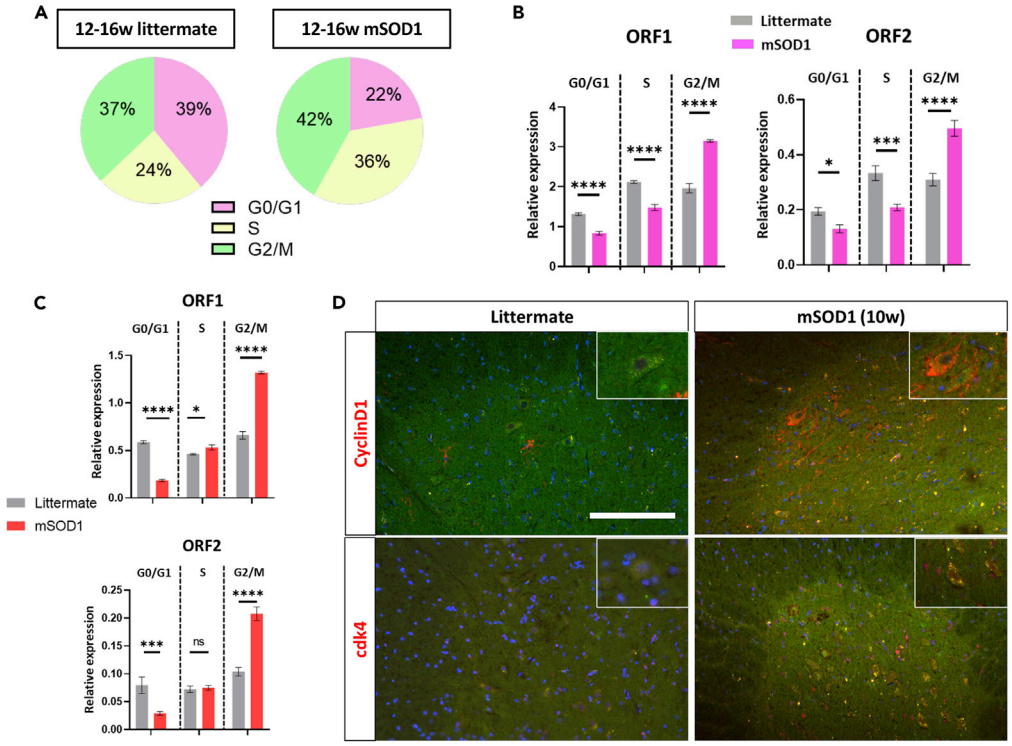

Figure 6. Cell cycle-dependent L1 upregulation in SC neurons of mSOD1 mouse

(A) SC neurons isolated from 12-16weeks-old mSOD1 mice or littermate control were incubated at 37°C with Hoechst33342 dye and cell cycle phase distributions of live neurons were analyzed by flow cytometer. Relative frequencies of neurons in each cell cycle phase (G0/G1, S, and G2/M) were quantified for mSOD1 or littermate mice. Representative data of three independent experiments with similar results are shown.

(B) Live SC neurons in G0/G1, S, or G2/M phases were sorted according to the gating predetermined via splenocyte analysis. Relative expression of ORF1 and ORF2 was quantified by qRT-PCR. Representative data of three independent experiments with similar results are shown. Statistical analysis was performed by two-way ANOVA with Bonferroni's multiple comparison. *, $p < 0.05$; **, $p < 0.01$; ***, $p < 0.001$; ****, $p < 0.0001$.

(C) Relative expression levels of ORF1 and ORF2 in mSOD1 or littermate neurons of either G0/G1, S, G2/M phases in (B) were normalized based on their frequency as quantified in (A). Statistical analysis was performed by two-way ANOVA with Bonferroni's multiple comparison.

(D) Immunofluorescence images of SC section obtained from 10-week old mSOD1 mice or littermate controls were stained with anti-ORF1 Ab, anti-Cdk4 Ab, and anti-Cyclin D1 Ab. (Inset) Fluorescence images of Cdk4-or Cyclin D1-positive cells with higher magnification. Representative data of two independent experiments with similar results are shown. Bars, 200 μm.

immunospot (ELISpot) assay. As shown in Figure 7A, EAE-derived CNS Th cells stimulated by presented ORF1 peptides generated significantly higher numbers of granzyme B spots than those cocultured without ORF1 protein presentation. Few granzyme B-secreting cells were observed amongst splenic Th cells with no difference between the presence or absence of ORF1 presentation (Figure 7A). Therefore, SC -infiltrating Th cells during EAE could recognize and respond to ORF1 presented peptides leading to degranulation and granzyme B secretion.

Next, we used this system to examine a role for ORF1-induced priming of CNS Th cells to produce granzyme B in ND in mSOD1 mice. CNS Th cells stimulated with ORF1-pulsed BMDC resulted in significantly higher numbers of granzyme B spots than those cocultured with intact BMDCs (Figure 7B). Similar results were obtained in 5×FAD mouse-derived CNS Th cells, which also showed augmented ORF-1-dependent granzyme B secretion (Figure 7C). Interestingly, whole CNS Th cells from 5xFAD mouse provided more granzyme B spots if stimulated with immobilized anti-CD3 antibody compared with ORF-1 presentation (Figure S10), suggesting that other ectopically expressed antigens may also be involved in the activation of populations of neurotoxic CNS Th cells under chronic inflammation.

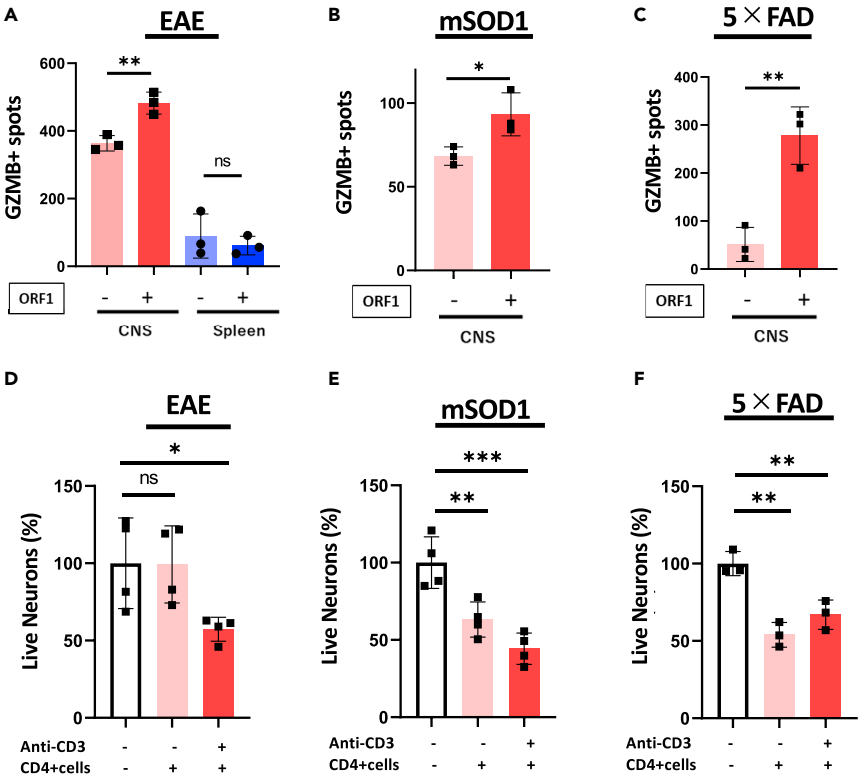

Figure 7. ORF1-primed granzyme B secretion and neurotoxicity by CNS Th cell

(A) $CD4^+$ T cells isolated from SC of EAE mice (day 28) were incubated with BMDCs preloaded with or without *in vitro* transcribed/translated ORF1 protein for 72 h. Granzyme B-secreting $CD4^+$ T cells were quantified by ELISpot. Numerated data (n = 3) from three independent experiments with similar results are shown. *, $p < 0.05$; **, $p < 0.01$; ***, $p < 0.001$; ****, $p < 0.0001$.

(B) $CD4^+$ T cells isolated from SC of 16weeks-old mSOD1 mice were incubated with BMDCs preloaded with or without ORF1 protein for 72 h. Granzyme B-secreting $CD4^+$ T cells were quantified by ELISpot. Representative data (n = 3) from three independent experiments are shown.

(C) $CD4^+$ T cells isolated from whole brain of 15m-old 5xFAD mice were incubated with BMDCs preloaded with ORF1 protein for 72 h. Granzyme B-secreting $CD4^+$ T cells were quantified by ELISpot. Representative data (n = 3) from three independent experiments with similar results are shown.

(D) $CD4^+$ T cells isolated from CNS of EAE mice (day 28) were incubated with embryonic hippocampal neurons with or without anti-CD3 stimulation for 72 h. The number of viable cells was determined by quantifying ATP luminescence. Numerated data (n = 4) from three independent experiments with similar results are shown.

(E) $CD4^+$ T cells isolated from SCs of SOD mice (16w) were incubated with embryonic hippocampal neurons with or without anti-CD3 stimulation for 72 h. The number of viable cells was determined by quantifying ATP luminescence. Numerated data (n = 4) from three independent experiments with similar results are shown.

(F) $CD4^+$ T cells isolated from CNS of 5×FAD mice (12m) were incubated with embryonic hippocampal neurons with or without anti-CD3 stimulation for 72 h. The number of viable cells was determined by quantifying ATP luminescence. Numerated data (n = 3) from three independent experiments with similar results are shown. Statistical analysis was performed by unpaired Student's *t* test.

To further confirm the direct neurotoxicity of CNS Th cells, hippocampal primary neurons were cocultured with CNS Th cells obtained from EAE, mSOD1 or 5xFAD mice. As shown in Figures 7D–7F, CNS Th cells generated significant cytotoxicity with or without further stimulation by anti-CD3 antibody. Similarly, the neurotoxic activity of CNS Th cells from 5xFAD mice was abolished in Th cells from granzyme B-deficient 5xFAD mice (Figure S11). Considering that almost all granzyme-expressing Th cells are found within the Eomes-positive subset (Figure S1), the Eomes + Th subset is more cytotoxic against neurons than Eomes- Th cells. In summary, Eomes + Th cells play a pathogenic role in neurodegeneration that depends on granzyme B secretion following recognition of ORF1 or additional proteins expressed in CNS. Therefore, the pathogenic triad of Eomes + T cells, L1-ORF1, and granzyme B may represent a previously unappreciated propagation mechanism of neurodegeneration that is lurking behind the cell-autonomous neuronal cell death.

DISCUSSION

Neurodegeneration is a process of crucial damage to neuronal structures and functions leading to clinical manifestations including cognitive impairment, motor ataxia, and other neurological deteriorations. Recent molecular genetic research has successfully unveiled a series of risk factors such as TDP-43, Amyloid β, and α-synuclein, which are schematically relevant to pathogenesis of ALS, AD, PD, respectively (Jucker and Walker, 2011). Meanwhile, glial activation during the clearance of such protein aggregates provokes chronic neuroinflammation to the extent that immune responses in the CNS are compromised. Thus non-cell autonomous pathogenesis beyond the CNS must be considered to understand the elusive and entangled process of neurodegeneration. In particular, neurodegeneration is not necessarily specific to typical NDs and similar neurodegeneration-related pathology is apparent in chronic neuroinflammatory diseases such as SPMS. We have recently revealed that Eomes + Th cells play a pivotal role for neurodegeneration in late EAE (Raveney et al., 2015) and in SPMS (Raveney et al., 2021). In such cases, a chronic inflammatory milieu gives rise to the ectopic expression of the transcription factor Eomes and confers Th cells with granzyme B-mediated neurotoxicity capabilities (Zhang et al., 2019). In this manuscript, we demonstrate that the neurotoxic Th cells generated in the inflamed CNS constitute a key population in a wide range of neurodegenerative disease via ORF1-mediated priming, leading to the secretion of neurotoxic granzyme B.

Approximately 45% of the human genome is composed of transposable elements (TE) and L1 consists of one-third of such TE (Richardson et al., 2014; Thomas et al., 2012). Some L1s are still retrotransposition-competent and L1 mobilization is one of the major causes of neurodevelopmental and neurodegenerative disorders (Apicco et al., 2018; Frost et al., 2014; Prudencio et al., 2017). The frequency of retrotransposition is, however, not necessarily high enough to explain the pathogenic link to all processes of neurodegeneration, and the pathogenic involvement of TEs in diverse neurodegenerative diseases remains enigmatic. Intriguingly, recent reports showed that a subtype of ALS neurons were strongly associated with activation marks of TE and the loss of nuclear TDP-43 is associated with L1 derepression (Liu et al., 2019; Tam et al., 2019), suggesting that activation of TE does not merely result from bystander effects, but constitutes an intrinsic element for pathogenesis of neurodegeneration. Due to detrimental consequences, L1 expression is strongly suppressed in quiescent somatic cells and derepressed via inflammation-elicited and cell division-associated epigenetic modification in tumor cells and neural stem/progenitor cells, respectively. Although a set of TEs are constitutively expressed in medullary thymic epithelial cells (Larouche et al., 2020), it seems that this is not enough to fully establish immunological tolerance against numbers of TEs expressed during inflammation (Carter et al., 2020; Kong et al., 2019). Such potent immunogenic properties of L1 prompt examine prototypic antigen(s) that enable the manipulation of clinical signs of neurodegeneration. As a consequence, we have recently demonstrated that Eomes + Th cells accumulate in the CNS of late EAE and in the SPMS brain (Raveney et al., 2015, 2021).

Interestingly, the disease-associated accumulation of Eomes + Th cells is recapitulated in the CNS of mSOD1 and 5xFAD mice, which secrete neurotoxic granzyme B upon stimulation with ORF1 antigen(s) as well as EAE-derived CNS Th cells. These results suggest that the accumulation of Eomes + Th cells in the CNS and their subsequent ORF1-dependent secretion of granzyme B is a common feature of Th cells during neuroinflammation that leads to diverse neurodegeneration. Granzyme B, an apoptosis-prone serine protease stored in the granules of cytolytic immune cells, such as natural killer (NK) cells and cytotoxic T cells, damages neurons in cerebral ischemia or spinal cord injury. It cleaves caspases-3/7, poly ADP ribose polymerase (Parp), Bid, and mitochondrial respiratory complex I subunits including V1, S1, and S2 (Lionello et al., 2020; Martinvalet, 2019) to induce neuronal cell death. Importantly, caspase-3 cleavage potentiates propagation of granzyme B-mediated apoptotic pathway via perpetuation of a mitochondrial amplification loop (Metkar et al., 2003). As caspase-3 promotes neurodegeneration in mSOD1 mice (Li et al., 2000), the mitochondria-targeting commonality between granzyme B and mSOD1 makes it difficult to distinguish individual pathogenic involvement of each which then manifests as clinical signs. Therefore, further investigation is needed to clarify the mechanism of granzyme B-mediated pathogenesis in neurodegeneration.

Aberrant L1 activation is reported in diverse neurodegenerative disorders including AD, ALS, Progressive Supranuclear Palsy, and Frontotemporal lobar degeneration (Ochoa Thomas et al., 2020; Terry and Devine, 2019). We confirmed neuronal L1 upregulation both in late EAE and the mSOD1 mouse and the kinetics of L1 expression is well correlated with disease onset and progression. Modes of L1 derepression seem intrinsically different between individual disease models of neurodegeneration. During EAE pathogenesis, Foxa1-mediated chromatin relaxation, AhR-dependent active transcription and premature polyadenylation limit

the transcription of retrotransposition-competent L1, whereas neuronal L1 induction in mSOD1 mice with prolonged and progressive neurodegeneration depends on cell cycle progression. As Foxa1 is a pioneer transcription factor that modulates the chromatin accessibility landscape (Glont et al., 2019; Zhang et al., 2016) and epigenetic modification is implicated in several neurodegenerative diseases (Berson et al., 2018), the neuronal genetic/epigenetic landscape that allow ectopic L1 activation under neurodegeneration should be studied via single cell ChIP-Seq analysis. Most importantly, a series of events take place in advance of clinical signs of neurodegeneration, suggesting that they may be critically involved in the pathogenesis of neurodegeneration. Significant numbers of live SC neurons are in S to G_2/M phase, even in normal mice and such skewed cell cycle progression is further apparent in mSOD1 mice. The high frequency of SC neurons in cell cycle progression is comparable with that observed in mature adult human neurons in health or neurodegenerative disease (Pack et al., 2005) and those aneuploid neurons are functionally active and form neural circuitries in the brain (Kingsbury et al., 2005). Notably, incomplete cell cycle progression and subsequent aneuploidy are commonly observed in neurons from diverse neurodegenerative diseases such as AD, ALS, glaucoma and PD (Joseph et al., 2020), conferring vulnerability to cell death by mitotic catastrophe amongst neurons (Vitale et al., 2011) and other cell cycle checkpoint failure.

Interestingly, our data suggest that neurons in G_2/M phase show relatively higher L1 expression and that cell cycle progression plays a crucial role for unintended L1 expression in neurons and this cell cycle reentry allows ectopic L1 transcription in mature neurons, which leads to occasional neurodegeneration. Considering the longer disease duration of human diseases, both active and cell cycle-mediated mechanisms of L1 upregulation must be in operation in the case of authentic SPMS. Moreover, both mutant SOD1 (G93A) protein and Aβ oligomer have been demonstrated to promote cell cycle progression (Cova et al., 2010; Varvel et al., 2008) suggesting that previously unappreciated properties of these proteins may be intrinsic to the pathogenesis of neurodegeneration. Meanwhile, retrotransposition is associated with cell division or cell cycle progression (Mita et al., 2018; Shi et al., 2007) and we also observed transcriptional upregulation of ORF2 and L1-GFP + neurons in the SC of mSOD1 mice. However, L1 retrotransposition in post-mitotic neurons was only observed in experimental settings *in vitro* (Macia et al., 2017) and our data quantifying ORF1 and ORF2 by RT-PCR support this finding, with ORF1 transcript increased over ORF2 (Figure 6B). L1 retrotransposition is associated with genomic instability in many aspects of cellular responses (Kazazian and Goodier, 2002); therefore, it may affect or determine the vulnerability of retrotransposed neurons to cell death. Further investigation is required to clarify how L1 retrotransposition *per se* is involved in the pathogenesis of neurodegeneration.

Collectively, our data suggest that the accumulation of Eomes + Th cells in the CNS and aberrant L1 expression in neurons are commonly observed during the process of neurodegeneration in diverse disease models. The pathogenic involvement of L1 has been reported in terms of retrotransposition and follows genomic instability or aberrant gene expression. Therefore, as far as the authors are aware this is the first demonstration of a retrotransposition-independent adverse effect of L1, in which ORF1 encoded by truncated transcripts induce pathogenic consequences in coordination with other coexisting components such as Eomes + Th cells. Although the mode of L1 expression is diverse in different disease models, the Th cells infiltrating CNS tissues secrete neurotoxic granzyme B upon encounter with ORF1 protein, which provokes further cell death of neighboring neurons. This results in further supply of ORF1 from the dying neurons and so establishes a vicious cycle of immune-mediated neuronal cell death, leading to the propagation of neurodegeneration. Considering that the immune-mediated neurotoxicity is set in motion after a supply of antigen(s), it is conceivable that neuron-autonomous cell death ignites this vicious cycle in its earliest phase and Eomes + Th cells distributed in the vicinity of such dying neurons may damage surrounding neurons via secretion of granzyme B, leading to a prolonged propagation of neurodegeneration. Therefore, cell-autonomous and immune cell-mediated neuronal cell death may form two sides of the same coin that work together for initiation and progression of neurodegeneration.

Limitation of the study

In this study, we revealed an immune-mediated vicious cycle of neurotoxicity that is common in diverse animal models of neurodegeneration. To enhance the value of our findings, further investigation is essential to demonstrate the pathogenic significance of this immune-mediated neurodegeneration. Namely, any improvement of clinical symptoms of neurodegeneration after therapeutic intervention targeting this immune-mediated pathogenesis should be investigated by employing appropriate animal models of neurodegenerative diseases.

STAR★METHODS

Detailed methods are provided in the online version of this paper and include the following:

- KEY RESOURCES TABLE
- RESOURCE AVAILABILITY
  - Lead contact
  - Materials availability
  - Data and code availability
- EXPERIMENTAL MODEL AND SUBJECT DETAILS
  - Mice, EAE induction and scoring
- METHOD DETAILS
  - Flow cytometry analysis
  - Adult neuron isolation and siRNA treatment
  - RNA extraction and qRT-PCR
  - Immunofluorescence imaging
  - Kynurenine quantification
  - Cell cycle analysis
  - ELISpot assay
  - Neurotoxicity assay
- QUANTIFICATION AND STATISTICAL ANALYSIS

SUPPLEMENTAL INFORMATION

Supplemental information can be found online at https://doi.org/10.1016/j.isci.2022.104278.

ACKNOWLEDGMENTS

We are grateful to Dr. Okamura (National Center for Global Health and Medicine (NCGM), Tokyo, Japan) for providing L1-GFP mice. We thank A. Takeo, C. Koto, and K. Inoue for excellent technical assistance and animal care. This work was supported by JSPS KAKENHI Grant Numbers 20K07895 (S.O.)/18H04045 (T.Y.), National Institute of Neuroscience Intramural Research Grant for Neurological and Psychiatric Disorders 30-5/1-4/3-5 (S.O.) and the Mitsubishi Foundation Research Grants in the Natural Sciences (S.O.).

AUTHOR CONTRIBUTIONS

Conceptualization, C.Z., T.Y., and S.O.; Methodology, F.T., C.Z., H.H., and S.O.; Investigation, F.T., C.Z., and B.R.; Writing – Original Draft, F.T. and S.O.; Writing –Review & Editing, C.Z., B.R., T.Y., N.H., and S.O.; Funding Acquisition, T.Y. and S.O.; Resources, T.Y. and S.O.; Supervision, T.Y., N.H., and S.O.

DECLARATION OF INTERESTS

The authors declare no competing financial interests.

Received: November 5, 2021
Revised: March 25, 2022
Accepted: April 18, 2022
Published: May 20, 2022

REFERENCES

Apicco, D.J., Ash, P.E.A., Maziuk, B., LeBlang, C., Medalla, M., Al Abdullatif, A., Ferragud, A., Botelho, E., Ballance, H.I., Dhawan, U., et al. (2018). Reducing the RNA binding protein TIA1 protects against tau-mediated neurodegeneration in vivo. Nat. Neurosci. *21*, 72–80. https://doi.org/10.1038/s41593-017-0022-z.

Berson, A., Nativio, R., Berger, S.L., and Bonini, N.M. (2018). Epigenetic regulation in neurodegenerative diseases. Trends Neurosci. *41*, 587–598. https://doi.org/10.1016/j.tins.2018.05.005.

Carter, V., LaCava, J., Taylor, M.S., Liang, S.Y., Mustelin, C., Ukadike, K.C., Bengtsson, A., Lood, C., and Mustelin, T. (2020). High prevalence and disease correlation of autoantibodies against p40 encoded by long interspersed nuclear elements in systemic lupus erythematosus. Arthritis Rheumatol. *72*, 89–99. https://doi.org/10.1002/art.41054.

Ciccocioppo, F., Bologna, G., Ercolino, E., Pierdomenico, L., Simeone, P., Lanuti, P., Pieragostino, D., Del Boccio, P., Marchisio, M., and Miscia, S. (2020). Neurodegenerative diseases as proteinopathies-driven immune disorders. Neural Regen. Res. *15*, 850–856. https://doi.org/10.4103/1673-5374.268971.

Correale, J., Gaitan, M.I., Ysrraelit, M.C., and Fiol, M.P. (2017). Progressive multiple sclerosis: from pathogenic mechanisms to treatment. Brain *140*, aww258–aww546. https://doi.org/10.1093/brain/aww258.

Cova, E., Ghiroldi, A., Guareschi, S., Mazzini, G., Gagliardi, S., Davin, A., Bianchi, M., Ceroni, M., and Cereda, C. (2010). G93A SOD1 alters cell cycle in a cellular model of amyotrophic lateral

sclerosis. Cell. Signal. *22*, 1477–1484. https://doi.org/10.1016/j.cellsig.2010.05.016.

G. Cristofari, ed. (2017). Human Retrotransposons in Health and Disease (Springer).

De Cecco, M., Ito, T., Petrashen, A.P., Elias, A.E., Skvir, N.J., Criscione, S.W., Caligiana, A., Brocculi, G., Adney, E.M., Boeke, J.D., et al. (2019). L1 drives IFN in senescent cells and promotes age-associated inflammation. Nature *566*, 73–78. https://doi.org/10.1038/s41586-018-0784-9.

Deczkowska, A., Keren-Shaul, H., Weiner, A., Colonna, M., Schwartz, M., and Amit, I. (2018). Disease-associated microglia: a Universal immune sensor of neurodegeneration. Cell *173*, 1073–1081. https://doi.org/10.1016/j.cell.2018.05.003.

Frost, B., Hemberg, M., Lewis, J., and Feany, M.B. (2014). Tau promotes neurodegeneration through global chromatin relaxation. Nat. Neurosci. *17*, 357–366. https://doi.org/10.1038/nn.3639.

Glont, S.E., Chernukhin, I., and Carroll, J.S. (2019). Comprehensive genomic analysis reveals that the pioneering function of FOXA1 is independent of hormonal signaling. Cell Rep. *26*, 2558–2565.e3. https://doi.org/10.1016/j.celrep.2019.02.036.

Hohjoh, H., and Singer, M.F. (1996). Cytoplasmic ribonucleoprotein complexes containing human LINE-1 protein and RNA. EMBO J. *15*, 630–639. https://doi.org/10.1002/j.1460-2075.1996.tb00395.x.

Hohjoh, H., and Singer, M.F. (1997). Sequence-specific single-strand RNA binding protein encoded by the human LINE-1 retrotransposon. EMBO J. *16*, 6034–6043. https://doi.org/10.1093/emboj/16.19.6034.

Ishak, C.A., Marshall, A.E., Passos, D.T., White, C.R., Kim, S.J., Cecchini, M.J., Ferwati, S., MacDonald, W.A., Howlett, C.J., Welch, I.D., et al. (2016). An RB-EZH2 complex mediates silencing of repetitive DNA sequences. Mol. Cell *64*, 1074–1087. https://doi.org/10.1016/j.molcel.2016.10.021.

Joseph, C., Mangani, A.S., Gupta, V., Chitranshi, N., Shen, T., Dheer, Y., Mirzaei, M., You, Y., Graham, S.L., and Gupta, V. (2020). Cell cycle deficits in neurodegenerative disorders: uncovering molecular mechanisms to drive innovative therapeutic development. Aging Dis. *11*, 946–966. https://doi.org/10.14336/AD.2019.0923.

Jucker, M., and Walker, L.C. (2011). Pathogenic protein seeding in Alzheimer disease and other neurodegenerative disorders. Ann. Neurol. *70*, 532–540. https://doi.org/10.1002/ana.22615.

Kappos, L., Bar-Or, A., Cree, B.A.C., Fox, R.J., Giovannoni, G., Gold, R., Arnold, D.L., Arnould, S., Scherz, T., Wolf, C., et al. (2018). Siponimod versus placebo in secondary progressive multiple sclerosis (EXPAND): a double-blind, randomised, phase 3 study. Lancet *391*, 1263–1273. https://doi.org/10.1016/s0140-6736(18)30475-6.

Kazazian, H.H., Jr., and Goodier, John L. (2002). LINE drive: retrotransposition and genome instability. Cell *110*, 277–280.

Keren-Shaul, H., Spinrad, A., Weiner, A., Matcovitch-Natan, O., Dvir-Szternfeld, R., Ulland, T.K., David, E., Baruch, K., Lara-Astaiso, D., Toth, B., et al. (2017). A unique microglia type associated with restricting development of Alzheimer's disease. Cell *169*, 1276–1290.e17. https://doi.org/10.1016/j.cell.2017.05.018.

Kingsbury, M.A., Friedman, B., McConnell, M.J., Rehen, S.K., Yang, A.H., Kaushal, D., and Chun, J. (2005). Aneuploid neurons are functionally active and integrated into brain circuitry. Proc. Natl. Acad. Sci. U S A, 6143–6147. https://doi.org/10.1073/pnas.0408171102.

Kolosha, V.O., and Martin, S.L. (2003). High-affinity, non-sequence-specific RNA binding by the open reading frame 1 (ORF1) protein from long interspersed nuclear element 1 (LINE-1). J. Biol. Chem. *278*, 8112–8117. https://doi.org/10.1074/jbc.M210487200.

Kong, Y., Rose, C.M., Cass, A.A., Williams, A.G., Darwish, M., Lianoglou, S., Haverty, P.M., Tong, A.J., Blanchette, C., Albert, M.L., et al. (2019). Transposable element expression in tumors is associated with immune infiltration and increased antigenicity. Nat. Commun. *10*, 5228. https://doi.org/10.1038/s41467-019-13035-2.

Kwidzinski, E., and Bechmann, I. (2007). Ido expression in the brain: a double-edged sword. J. Mol. Med. (Berl) *85*, 1351–1359. https://doi.org/10.1007/s00109-007-0229-7.

Larouche, J.D., Trofimov, A., Hesnard, L., Ehx, G., Zhao, Q., Vincent, K., Durette, C., Gendron, P., Laverdure, J.P., Bonneil, E., et al. (2020). Widespread and tissue-specific expression of endogenous retroelements in human somatic tissues. Genome Med. *12*, 40. https://doi.org/10.1186/s13073-020-00740-7.

Li, M., Ona, V.O., Guégan, C., Chen, M., Jackson-Lewis, V., Andrews, L.J., Olszewski, A.J., Stieg, P.E., Lee, J.P., Przedborski, S., et al. (2000). Functional role of caspase-1 and caspase-3 in an ALS transgenic mouse model. Science. https://doi.org/10.1126/science.288.5464.335.

Lionello, S., Marzaro, G., and Martinvalet, D. (2020). SAM50, a side door to the mitochondria: the case of cytotoxic proteases. Pharmacol. Res. *160*, 105196. https://doi.org/10.1016/j.phrs.2020.105196.

Liu, E.Y., Russ, J., Cali, C.P., Phan, J.M., Amlie-Wolf, A., and Lee, E.B. (2019). Loss of nuclear TDP-43 is associated with decondensation of LINE retrotransposons. Cell Rep. *27*, 1409–1421.e6. https://doi.org/10.1016/j.celrep.2019.04.003.

Macia, A., Widmann, T.J., Heras, S.R., Ayllon, V., Sanchez, L., Benkaddour-Boumzaouad, M., Munoz-Lopez, M., Rubio, A., Amador-Cubero, S., Blanco-Jimenez, E., et al. (2017). Engineered LINE-1 retrotransposition in nondividing human neurons. Genome Res. *27*, 335–348. https://doi.org/10.1101/gr.206805.116.

Martinvalet, D. (2019). Mitochondrial entry of cytotoxic proteases: a new insight into the granzyme B cell death pathway. Oxid. Med. Cell. Longev. 1–13. https://doi.org/10.1155/2019/9165214.

Mathys, H., Adaikkan, C., Gao, F., Young, J.Z., Manet, E., Hemberg, M., De Jager, P.L., Ransohoff, R.M., Regev, A., and Tsai, L.H. (2017). Temporal tracking of microglia activation in neurodegeneration at single-cell resolution. Cell Rep. *21*, 366–380. https://doi.org/10.1016/j.celrep.2017.09.039.

Metkar, S.S., Wang, B., Ebbs, M.L., Kim, J.H., Lee, Y.J., Raja, S.M., and Froelich, C.J. (2003). Granzyme B activates procaspase-3 which signals a mitochondrial amplification loop for maximal apoptosis. J. Cell Biol. *160*, 875–885. https://doi.org/10.1083/jcb.200210158.

Mita, P., Wudzinska, A., Sun, X., Andrade, J., Nayak, S., Kahler, D.J., Badri, S., LaCava, J., Ueberheide, B., Yun, C.Y., et al. (2018). LINE-1 protein localization and functional dynamics during the cell cycle. Elife *7*. https://doi.org/10.7554/eLife.30058.

Nicole, A., Suarez, A.M., and Muotri, A.R. (2017). LINE-1 retrotransposons in healthy and diseased human brain. Dev. Neurobiol. *78*, 434–455.

Ochoa Thomas, E., Zuniga, G., Sun, W., and Frost, B. (2020). Awakening the dark side: retrotransposon activation in neurodegenerative disorders. Curr. Opin. Neurobiol. *61*, 65–72. https://doi.org/10.1016/j.conb.2020.01.012.

Okudaira, N., Goto, M., Yanobu-Takanashi, R., Tamura, M., An, A., Abe, Y., Kano, S., Hagiwara, S., Ishizaka, Y., and Okamura, T. (2011). Involvement of retrotransposition of long interspersed nucleotide element-1 in skin tumorigenesis induced by 7,12-dimethylbenz[a] anthracene and 12-O-tetradecanoylphorbol-13-acetate. Cancer Sci. *102*, 2000–2006. https://doi.org/10.1111/j.1349-7006.2011.02060.x.

Okudaira, N., Iijima, K., Koyama, T., Minemoto, Y., Kano, S., Mimori, A., and Ishizaka, Y. (2010). Induction of long interspersed nucleotide element-1 (L1) retrotransposition by 6-formylindolo[3,2-b]carbazole (FICZ), a tryptophan photoproduct. Proc. Natl. Acad. Sci. U S A *107*, 18487–18492. https://doi.org/10.1073/pnas.1001252107.

Pack, S.D., Weil, R.J., Vortmeyer, A.O., Zeng, W., Li, J., Okamoto, H., Furuta, M., Pak, E., Lubensky, I.A., Oldfield, E.H., and Zhuang, Z. (2005). Individual adult human neurons display aneuploidy: detection by fluorescence in situ hybridization and single neuron PCR. Cell Cycle *4*, 1758–1760. https://doi.org/10.4161/cc.4.12.2153.

Peze-Heidsieck, E., Bonnifet, T., Znaidi, R., Ravel-Godreuil, C., Massiani-Beaudoin, O., Joshi, R.L., and Fuchs, J. (2021). Retrotransposons as a source of DNA damage in neurodegeneration. Front. Aging Neurosci. *13*, 786897. https://doi.org/10.3389/fnagi.2021.786897.

Prudencio, M., Gonzales, P.K., Cook, C.N., Gendron, T.F., Daughrity, L.M., Song, Y., Ebbert, M.T., van Blitterswijk, M., Zhang, Y.J., Jansen-West, K., et al. (2017). Repetitive element transcripts are elevated in the brain of C9orf72 ALS/FTLD patients. Hum. Mol. Genet. *26*, 3421–3431. https://doi.org/10.1093/hmg/ddx233.

Przedborski, S., Vila, M., and Jackson-Lewis, V. (2003). Series introduction: neurodegeneration: what is it and where are we? J. Clin. Invest. *111*, 3–10. https://doi.org/10.1172/jci200317522.

Raine, C.S. (2000). Inflammation in Alzheimer's disease: a view from the periphery. Neurobiol. Aging *21*, 437–440.

Ranganathan, S., and Bowser, R. (2003). Alterations in G(1) to S phase cell-cycle regulators during amyotrophic lateral sclerosis. Am. J. Pathol. *162*, 823–835.

Ravel-Godreuil, C., Znaidi, R., Bonnifet, T., Joshi, R.L., and Fuchs, J. (2021). Transposable elements as new players in neurodegenerative diseases. FEBS Lett. *595*, 2733–2755. https://doi.org/10.1002/1873-3468.14205.

Raveney, B.J.E., Oki, S., Hohjoh, H., Nakamura, M., Sato, W., Murata, M., and Yamamura, T. (2015). Eomesodermin-expressing T-helper cells are essential for chronic neuroinflammation. Nat. Commun. *6*, 8437. https://doi.org/10.1038/ncomms9437.

Raveney, B.J.E., Sato, W., Takewaki, D., Zhang, C., Kanazawa, T., Lin, Y., Okamoto, T., Araki, M., Kimura, Y., Sato, N., et al. (2021). Involvement of cytotoxic Eomes-expressing CD4(+) T cells in secondary progressive multiple sclerosis. Proc. Natl. Acad. Sci. U S A *118*. https://doi.org/10.1073/pnas.2021818118.

Richardson, S.R., Morell, S., and Faulkner, G.J. (2014). L1 retrotransposons and somatic mosaicism in the brain. Annu. Rev. Genet. *48*, 1–27. https://doi.org/10.1146/annurev-genet-120213-092412.

Rovaris, M., Confavreux, C., Furlan, R., Kappos, L., Comi, G., and Filippi, M. (2006). Secondary progressive multiple sclerosis: current knowledge and future challenges. Lancet Neurol. *5*, 343–354. https://doi.org/10.1016/s1474-4422(06)70410-0.

Seol, Y., Ki, S., Ryu, H.L., Chung, S., Lee, J., and Ryu, H. (2020). How microglia manages non-cell autonomous vicious cycling of Aβ toxicity in the pathogenesis of AD. Front. Mol. Neurosci. *13*, 593724. https://doi.org/10.3389/fnmol.2020.593724.

Shi, X., Seluanov, A., and Gorbunova, V. (2007). Cell divisions are required for L1 retrotransposition. Mol. Cell Biol. *27*, 1264–1270. https://doi.org/10.1128/MCB.01888-06.

Smith, C.C., Selitsky, S.R., Chai, S., Armistead, P.M., Vincent, B.G., and Serody, J.S. (2019). Alternative tumour-specific antigens. Nat. Rev. Cancer *19*, 465–478. https://doi.org/10.1038/s41568-019-0162-4.

Tam, O.H., Rozhkov, N.V., Shaw, R., Kim, D., Hubbard, I., Fennessey, S., Propp, N., Fagegaltier, D., Ostrow, L.W., Phatnani, H., et al. (2019). Postmortem cortex samples identify distinct molecular subtypes of ALS: retrotransposon activation, oxidative stress, and activated glia. Cell Rep. *29*, 1164–1177.e5. https://doi.org/10.1016/j.celrep.2019.09.066.

Teneng, I., Stribinskis, V., and Ramos, K.S. (2007). Context-specific regulation of LINE-1. Genes Cells *12*, 1101–1110. https://doi.org/10.1111/j.1365-2443.2007.01117.x.

Terry, D.M., and Devine, S.E. (2019). Aberrantly high levels of somatic LINE-1 expression and retrotransposition in human neurological disorders. Front. Genet. *10*, 1244. https://doi.org/10.3389/fgene.2019.01244.

Thomas, C.A., Paquola, A.C., and Muotri, A.R. (2012). LINE-1 retrotransposition in the nervous system. Annu. Rev. Cell Dev. Biol. *28*, 555–573. https://doi.org/10.1146/annurev-cellbio-101011-155822.

Van Harten, A.C.M., Phatnani, H., and Przedborski, S. (2021). Non-cell-autonomous pathogenic mechanisms in amyotrophic lateral sclerosis. Trends Neurosci. *44*, 658–668. https://doi.org/10.1016/j.tins.2021.04.008.

Varvel, N.H., Bhaskar, K., Patil, A.R., Pimplikar, S.W., Herrup, K., and Lamb, B.T. (2008). Abeta oligomers induce neuronal cell cycle events in Alzheimer's disease. J. Neurosci. *28*, 10786–10793. https://doi.org/10.1523/JNEUROSCI.2441-08.2008.

Vitale, I., Galluzzi, L., Castedo, M., and Kroemer, G. (2011). Mitotic catastrophe: a mechanism for avoiding genomic instability. Nat. Rev. Mol. Cell Biol. *12*, 385–392. https://doi.org/10.1038/nrm3115.

Wu, Q., Mills, E.A., Wang, Q., Dowling, C.A., Fisher, C., Kirch, B., Fox, D.A., Mao-Draayer, Y., and Lundy, S.K. (2020). Siponimod enriches regulatory T and B lymphocytes in secondary progressive multiple sclerosis. JCI Insight *5*. https://doi.org/10.1172/jci.insight.134251.

Zhang, C., Raveney, B.J.E., Hohjoh, H., Tomi, C., Oki, S., and Yamamura, T. (2019). Extrapituitary prolactin promotes generation of Eomes-positive helper T cells mediating neuroinflammation. Proc. Natl. Acad. Sci. U S A *116*, 21131–21139. https://doi.org/10.1073/pnas.1906438116.

Zhang, Y., Zhang, D., Li, Q., Liang, J., Sun, L., Yi, X., Chen, Z., Yan, R., Xie, G., Li, W., et al. (2016). Nucleation of DNA repair factors by FOXA1 links DNA demethylation to transcriptional pioneering. Nat. Genet. *48*, 1003–1013. https://doi.org/10.1038/ng.3635.

STAR★METHODS

KEY RESOURCES TABLE

REAGENT or RESOURCE	SOURCE	IDENTIFIER
Antibodies		
Anti-CD4 (GK1.5) antibody	Bio Legend	Cat#100438; RRID:AB_11203718
Anti-CD8 (53-6.7) antibody	Bio Legend	Cat#100711; RRID: AB_312750
Anti-CD19 (1D3/CD19) antibody	Bio Legend	Cat#152406; RRID:AB_2629815
Anti-CD45 (30F11) antibody	Bio Legend	Cat#103154; RRID:AB_2572116
Anti-TCRβ (H57-597) antibody	Bio Legend	Cat# 109218, RRID:AB_493346
Anti-Eomes (Dan11Mag) antibody	Thermofisher	Cat#12-4875-82; RRID; AB_1603275
Anti-GZMB(QA16A02) antibody	Bio Legend	Cat#372206; RRID:AB_2687030
Anti-CD11c antibody	Bio Legend	Cat#117308; RRID; AB_313777
Anti-I-A antibody	Bio Legend	Cat#107631; RRID; AB_10900075
Anti-F4/80 antibody	Bio Legend	Cat#123118;RRID; AB_893477
anti-mouse CD16/CD32	Bio Legend	Cat#101301; RRID AB_312800
Anti-NeuN Ab Alexa Flour 488conjugate	Abcam	Cat#ab190195; RRID:AB_2716282
Anti-NeuN Ab Alexa Flour 647conjugate	Abcam	Cat#ab190565; RRID:AB_2716282
Anti-L1 ORF1p antibody	Novusbio	Cat#NBP2-66934
Alexa Fluor 647-conjugated Anti-Rabbit IgG	Jackson ImmunoResearch	Cat#211-605-109; AB_2339172
FITC-conjugated anti mouse IgG Fcγfragment specific	Jackson ImmunoResearch	Cat#115-096-071; AB_2338613
Anti-Olig2	biorbyt	Cat#orb680036
Alexa Fluor 488-conjugated anti-Olig2	Millipore	Cat#MABN50A4; AB_11205039
Alexa Fluor 647-conjugated anti-Iba1	Millipore	Cat#MABN92-AF647; RRID:AB_10917271
Anti-IBA1	LSBio	Cat#LS-C190046
Alexa Fluor 647-conjugated anti-GFAP	invitrogen	Cat#51-9792-82; RRID:AB_2762678
Alexa Fluor 488-conjugated anti-GFAP	invitrogen	Cat#53-9892-82; RRID:AB_10598515
Alexa Fluor 647-conjugated anti-Geminin	Santa Cruz	Cat#sc-74456 AF647; RRID:AB_1124963
Alexa Fluor 488-conjugated anti-Cdt1	Santa Cruz	Cat#sc-365305 AF488; RRID:AB_10847805
Alexa Fluor 647-conjugated anti-pRB1	Santa Cruz	Cat#sc-377540 AF647
anti-HNF-3α(A-3)	Santa Cruz	Cat#sc-514695
Hoechst33342	DOJINDO	Cat#346-07951
LIVE/DEAD™ Fixable Aqua Dead Cell Stain Kit	Thermofisher	Cat#L34957
LIVE/DEAD™ Fixable Near-IR Dead Cell Stain Kit	Thermofisher	Cat#L34975
Anti-E2F Alexa Fluor 647-conjugated antibody	Santa Cruz	Cat#sc-251 AF647; RRID:AB_627476
Anti-cdk4 Alexa Fluor 647-conjugated antibody	Santa Cruz	Cat#sc-23896 AF647; RRID:AB_627239
Anti-CyclinD1 Alexa Fluor 647-conjugated antibody	Santa Cruz	Cat#sc-8396 AF647; RRID:AB_627344
True Black Lipofuscin Auto fluorescence	BTI Biotum.Inc	Cat#23007
DAPI Fluoromount-G	Southern Biotech, USA	Cat#0100-20
Chemicals, peptides, and recombinant proteins		
Heat-killed *Mycobacterium tuberculosis* H37RA	Difco	Cat#231141
Incomplete Freund's adjuvant	Difco	Cat#DF0639-60-6
MOG35-55 peptide	Toray Research Center	N/A
Pertussis toxin	List Biological Laboratories	Cat#180
1-methyl-tryptophan; 1-MT	Sigma-Aldrich	Cat#MKCJ1127
MACS® adult brain dissociation kit	Miltenyi Biotech	Cat#130-107-677

(*Continued on next page*)

Continued

REAGENT or RESOURCE	SOURCE	IDENTIFIER
Non-neuron antibody-conjugated magnetic beads	Miltenyi Biotech	Cat#130-115-389
Dulbecco's Modified Eagle Medium	Gibco	Cat#12430-054
Cytoplasmic & Nuclear RNA purification Kit	Norgen Biotek	Cat#21000
RNeasy Mini Kit	Qiagen	Cat#74106
First-strand cDNA Kit	Takara Bio	Cat#RR036S
Prime Script IV 1 st atrand cDNA synthesis Mix Kit	Takara Bio	Cat#6215A
SYBR Green Master mix	Roche	Cat#06402712001
SEA BLOCK blocking buffer	Thermo Fisher	Cat#37527
Zenon Antibody Labeling Kit	Thermo Fishier	Cat#z25302
GM-CSF	R&D systems	Cat#415-ML-010
Lipopolysaccharide (LPS)	Nakarai	Cat#14877-94
IL-4	R&D systems	Cat#404-ML-010/CF
Poly-L-lysine hydrobromide	Sigma-Aldrich	Cat#P2636-100MG
Laminin	R&D systems	Cat#3400-010-02
TNT™ Quick Coupled Transcription/Translation System	Promega	Cat#PR-L1171
Kynurenine ELISA high sensitive kit	IDK	Cat#KR3728
Mouse CD4+/Granzyme B ELISpot Kit	R&D systems	Cat#EL6024
NeuroBrew-21	MACS	Cat#130-093-566
Neurobasal Medium	Milteny Biotec	Cat#130-093-570
Sodium Pyruvate	Gibco	Cat#11360-070
2-ME	Gibco	Cat#21985-023
Glutamax	Gibco	Cat#35050-061
anti-CD3(2C11)	Biolegend	Cat#100340; **RRID:AB_11149115**
CellTiter-Glo 2.0 reagent	Promega	Cat#G924B
Experimental models: Organisms/strains		
C57BL/6J	CLEA Japan, Inc	N/A
mSOD-1(G93A) mice	the Jackson Laboratory (Bar Harbor, MN)	N/A
5xFAD mice	the Jackson Laboratory (Bar Harbor, MN)	N/A
L1-GFP mice	Provided by Dr. Okamura (National Center for Global Health and Medicine (NCGM), Tokyo, Japan).	N/A
Oligonucleotides		
Foxa1 siRNA	Qiagen	Cat#1027416
Recombinant DNA		
L1 ORF1 expression vector	Hohjoh et al. EMBO J 16, 6034-6043 (1997)	N/A
Software and algorithms		
Prism	GraphPad	https://www.graphpad.com
BD FACSDiva	BD	http://www.bdbiosciences.com
FlowJo	BD	http://www.flowjo.com
Other		
FACS Canto II	BD Bioscience	N/A
FACS Aria liu	BD Bioscience	N/A
GentleMACS Octo Dissociator	Miltenyi Biotech	N/A
Real time PCRR instrument	Roche Diagnostics	LightCycler 96 instrument
Cryostat	Thermo Fisher	Cryostar NX70

(*Continued on next page*)

Continued

REAGENT or RESOURCE	SOURCE	IDENTIFIER
Promega Glomox MULTI DETECTION system	Promega	N/A
Fluorescence microscope	Keyence, Japan	BZ-X710
8-well LAB-TEK chambers	Nalge Nunc International	Cat#154534
Magnetofection NeuroMag	OZ BIOSCIENCES	N/A

RESOURCE AVAILABILITY

Lead contact

Further information and requests for resources and reagents should be directed to the lead contact, Shinji Oki (soki@ncnp.go.jp).

Materials availability

This paper does not report original materials.

All additional information about materials reported in this paper is available from the lead contact upon request.

Data and code availability

- Any additional information required to reanalyze the data reported in this study is available from the lead contact upon reasonable request.
- This paper does not report original code.

EXPERIMENTAL MODEL AND SUBJECT DETAILS

Mice, EAE induction and scoring

For EAE experiments, 6–8 weeks old mice were used. mSOD1 and 5xFAD mice were maintained up to 150 days and 15 months after birth, respectively. C57BL/6 mice were obtained from CLEA Japan, Inc. (Tokyo, Japan). mSOD-1(G93A) mice and 5xFAD mice were obtained from the Jackson Laboratory (Bar Harbor, MN). L1-GFP mice (Okudaira et al., 2011) were kindly provided by Dr. Okamura (National Center for Global Health and Medicine (NCGM), Tokyo, Japan).Both male and female animals were used in animal experiments and mice of each genotype were allocated randomly to different experiments. Mice were maintained in ventilated racks under a 12-h light/dark cycle with food and water *ad libitum* in temperature controlled, pathogen-free facilities. The breeding, the backcrossing and the maintenance of mice were performed at the animal facility of National Center of Neurology and Psychiatry (NCNP). All animal experiments in this study have been approved by the Animal Care and Use Committee of the National Institute of Neuroscience, NCNP, Japan (authorization number R3-53). All efforts were made to minimize suffering and to reduce the number of animals.

Mice, aged 6-9 weeks, were immunized subcutaneously with 100 μg MOG_{35-55} peptide (synthesized by Toray Research Center, Japan) emulsified in complete Freund's adjuvant containing 1 mg heat-killed *Mycobacterium tuberculosis* H37RA (Difco). The mice were injected intraperitoneally (i.p.) with 100 ng of pertussis toxin (List Biological Laboratories, USA) at the time of immunization and 2 days later. Manifestation of clinical symptoms of EAE were evaluated on a scale from 0 to 5 (0, no clinical signs; 0.5, tail weakness; 1, partial tail paralysis; 1.5, severe tail paralysis; 2, flaccid tail; 2.5, flaccid tail and hind limb weakness; 3, partial hind limb paralysis; 3.5, severe hind limb paralysis; 4, total hind limb paralysis; 4.5, hind and fore leg paralysis; 5, death). In some experiments, mice were intraperitoneally injected with IDO inhibitor (1-methyl-tryptophan; 1-MT, 5mg/mouse/day) (Sigma-Aldrich, USA) suspended in 2% starch PBS.

METHOD DETAILS

Flow cytometry analysis

Cells were treated with anti-mouse CD16/CD32 (BioLegend) for blocking Fc receptors and all staining procedures were performed in PBS containing 5% FCS. Dead cells were excluded using an Aqua Live/Dead fixable staining reagent (Invitrogen, USA). Monoclonal antibodies (anti-CD4 (GK1.5), anti-CD8 (53-6.7),

anti-CD19 (1D3/CD19), anti-CD45 (30F11), anti-Eomes (Dan11Mag), anti-TCRβ(H57-597) and anti-GZMB (QA16A02) were obtained from BioLegend or Therrmo-Fisher. Flow cytometry analysis was carried out by using a FACS Canto II cell analyzer (BD Biosciences) with a FACS Diva software and data were analyzed using a FlowJo software (BD BioSciences). For cell cycle analysis, neurons were stained with Hoechst33342 and the cells in individual cell cycle phases (G_0/G_1, S, and G_2/M) were sorted using a FACS Aria IIu cell sorter (BD BioSciences).

Adult neuron isolation and siRNA treatment

Spinal cords were digested with GentleMACS Octo Dissociator (Miltenyi Biotech) according to the manufacturer's instructions. Neurons were isolated by using MACS® adult brain dissociation kit (Miltenyi Biotech) with non-neuron antibody-conjugated magnetic beads. Isolated neurons were adjusted to maximum of 3.5×10^5 cells/mL in Dulbecco's Modified Eagle Medium (DMEM; Gibco) supplemented with 10% FCS. Typically, 200μL of cell suspension was seeded to 48 well plate coated with poly-L-lysine and laminin, and cultured at 37°C in a 5% CO2 atmosphere. Twenty-four hours later, cells were transfected with Foxa1 siRNA (10 nM each) by using Magnetofection NeuroMag kit (OZ BIOSCIENCES) and cultured up to 72hrs. Cells were harvested for RNA extraction, immunoblotting analysis and immunofluorescence imaging.

RNA extraction and qRT-PCR

Nuclear/cytoplasmic RNA, or total RNA were extracted from isolated neurons using a Cytoplasmic & Nuclear RNA purification Kit (Norgen Biotek), or RNeasy Mini Kit (Qiagen) according to the manufacturer's protocol. RNAs were reverse transcribed by using a first-strand cDNA Kit (Takara Bio, Japan) with random hexamer primers or Prime Script Ⅳ 1st strand cDNA synthesis Mix Kit (Takara Bio, Japan) with oligo-dT primers for qRT-PCR or premature polyadenylation analysis respectively. Gene expression was quantified by real-time qRT-PCR using a LightCycler 96 instrument (Roche Diagnostics, Japan) with SYBR Green Master mix (Roche). L1 transcripts were quantified by qRT-PCR with L1-TF primers targeting ORF1 and ORF2 (Cristofari, 2017). Primers obtained from Qiagen are listed in the STAR Methods.

Immunofluorescence imaging

For immunofluorescence imaging, SCs were fixed with 4% para-formaldehyde (PFA) for 24 h at 4°C and dissected by using a Cryostar NX70 cryostat (Thermo Fisher Scientific). Sections were dried, rehydrated, defatted and blocked with SEA BLOCK blocking buffer (Thermo Fisher Scientific) for 1h at room temperature. Specimens were incubated with fluorescence-conjugated primary antibodies and mounted using fluorescence mounting medium with DAPI (Southern Biotech, USA). All samples were imaged with a BZ-X710 automated fluorescence microscope (Keyence, Japan). The following antibodies were used; rabbit anti-L1 ORF1p (Novusbio, USA), Alexa Flour 488-conjugated rabbit anti-NeuN (Abcam), Alexa Fluor 647-conjugated Anti-Rabbit IgG (Jackson ImmunoResearch, USA) Alexa Fluor 647-conjugated rabbit anti-NeuN (Abcam)(1:200), anti-Olig2 (biorbyt)(1:50), Alexa Fluor 488-conjugated anti-Olig2 (Millipore)(1:50), Alexa Fluor 647-conjugated anti-Iba1 (Millipore, USA) (1:50), anti-IBA1 (LSBio, USA) (1:50), Alexa Fluor 647-conjugated anti-GFAP (invitrogen, USA) (1:50), Alexa Fluor 488-conjugated anti-GFAP (invitrogen, USA) (1:50), Alexa Fluor 647-conjugated anti-Rabbit IgG (Jackson ImmunoResearch, USA)(1:200). For cell cycle analysis, Alexa Fluor 647-conjugated anti-Geminin (Santa Cruz, USA)(1:50), Alexa Fluor 488-conjugated anti-Cdt1(Santa Cruz, USA)(1:50) and Alexa Fluor 647-conjugated anti-pRB1(Santa Cruz, USA)(1:50) were used. In some experiments, unconjugated antibodies were labeled with Alexa 488 or 647 fluorescent dye by using Zenon Antibody Labeling Kit (Thermo Fishier Scientific, USA).

For immunofluorescence imaging of cell culture, isolated adult neuronal cells were seeded in 8-well LAB-TEK chambers (Nalge Nunc International) after manual collagen coating. Cells were fixed with 1:1 Acetone/Methanol fixative for 20 min at −20°C, rinsed three times in PBS and blocked with Super BLOCK Blocking Buffer for 60 min at RT and incubated with primary antibody (anti-HNF-3αFOXA1(Santa Cruz, USA); 1:50) in SEA BLOCK Blocking Buffer for O/N at 4°C. After 3 times PBS wash, cells were incubated with FITC-conjugated anti mouse IgG Fcγfragment specific (Jackson ImmunoResearch)(1:200) and Alexa Flour 647-conjugated rabbit anti-NeuN (Abcam, USA)(1:200) for 2h at RT. In some experiments, samples were treated with True Black Lipofuscin Auto fluorescence (BTI, USA) before mounted with DAPI Fluoromount-G (Southen Biotech, USA) to suppress the autofluorescence signals.

Kynurenine quantification

The level of kynurenine in mouse spinal cords was quantified using a Kynurenine ELISA high sensitive kit (KR3728, IDK Germany) according to the manufacturer's instructions. Whole SCs isolated from either intact or EAE-induced B6 mice were homogenized by sonication on ice and centrifuged at 14,000g for 10 min at 4°C. The supernatants were subjected to quantification of kynurenine concentration.

Cell cycle analysis

Neurons isolated from SCs were stained with Hoechst 33342 (DOJINDO, Japan) for 30min, then staining with Live/Dead Near-IR Dead Cell Stain Kit (Invitrogen, USA) for 5 min at 37°C in CO2 incubator. The cells in individual cell cycle phases (G_0/G_1, S, and G_2/M) were sorted using a FACS Aria IIu cell sorter. As a reference for gate setting, spleen cells were similarly stained with Hoechst 33342 and analyzed (Figure S4A). RNAs extracted from individual sample were analyzed for expression of L1, Cdt1, and Geminin by qRT-PCR. Primers for Cdt1 and Geminin were obtained from Qiagen.

ELISpot assay

For *in vitro* expression of ORF-1 protein, full-length of ORF-1 was inserted into the expression plasmid pRSET vector (Invitrogen) as previously described (H. Hohjoh and Singer, 1996; Hirohiko Hohjoh and Singer, 1997). ORF-1 protein was translated *in vitro* using TNT T7 Quick Coupled Transcription/Translation System (Promega). The quality of expressed protein was determined using Transcend tRNA (Promega) and the protein size was confirmed on an conventional SDS-PAGE (Sodium dodecyl sulfate-polyacrylamide gel electrophoresis). Bone marrow cells obtained from B6 mice were cultured with DMEM supplemented with 20 ng/ml GM-CSF. Half volume of medium was replaced with that supplemented with fresh GM-CSF on day 3 and 6. On day 8, the floating and loosely attached cells were harvested. The recovered cells were stimulated with 100 ng/ml lipopolysaccharide (LPS) and 20 ng/ml IL-4 for 24 h. $CD11c^+$, MHC II^{hi}, $F4/80^-$ cells (BMDCs) were sorted and pulsed with ORF1 protein for 6-12 h. ORF1-loaded BMDCs and CNS-derived Th cells were incubated in the ELISpot plate precoated with both anti-CD4 Ab and anti-granzyme B Ab and subjected to quantification of granzyme B-producing cells using an ELISpot mouse CD4+/Granzyme B kit (R&D).

Neurotoxicity assay

For measuring neurotoxicity, embryonic mouse hippocampal neurons were picked up from E15.5 mouse brain and cultured for 24h in DMEM + medium at 37°C using 96 well flat bottom plate. Medium was changed to Neurobasal Medium (Miltenyi) supplemented with NeuroBrew-21(MACS), sodium pyruvate (Gibco) and 2-ME (Gibco) at days 2 and 3. After that, half of medium was changed to new medium every 3 days for 2 weeks. $CD4^+$ cells from CNS of each mouse (EAE; 5000 Th cells/well; SOD & FAD; 2000 Th cells/well) were co-cultured with embryonic neurons for 72 h at 37°C with or without anti-CD3 stimulation(1 μg/ml). The number of viable cells was determined by quantifying ATP using the CellTiter-Glo 2.0 (Promega) according to the manufacturer's instructions.

QUANTIFICATION AND STATISTICAL ANALYSIS

Statistical analysis was performed using Graphpad Prism 8 Software (GraphPad, USA) by applying unpaired Student's t test, one-way or two-way ANOVA with Bonferroni's multiple comparison as indicated. A p value <0.05 was considered as significant difference. ns, not significant; *, $p < 0.05$; **, $p < 0.01$; ***, $p < 0.001$; ****, $p < 0.0001$ throughout the manuscript.